A New Six-axis Load Cell. Part I: Design

Article *in* Experimental Mechanics · March 2011

DOI: 10.1007/s11340-010-9355-1

CITATIONS
48

READS
1,897

3 authors:

Giampiero Mastinu
Politecnico di Milano
139 PUBLICATIONS **1,665** CITATIONS
SEE PROFILE

Massimiliano Gobbi
Politecnico di Milano
171 PUBLICATIONS **1,641** CITATIONS
SEE PROFILE

Giorgio Previati
Politecnico di Milano
111 PUBLICATIONS **591** CITATIONS
SEE PROFILE

Experimental Mechanics
DOI 10.1007/s11340-010-9355-1

A New Six-axis Load Cell. Part I: Design

G. Mastinu · M. Gobbi · G. Previati

Received: 3 December 2009 / Accepted: 24 March 2010

Abstract A new high precision six-axis load cell is presented in two companion papers. The first paper (this one) is focused on the presentation of the load cell, the conceptual design, the modelling and the embodiment design. The second paper refers to the error analysis, the construction and the experimental assessment of the performances. The new load cell is able to measure the three components of both a force and a moment acting on the load cell itself. The sensing structural element of the six-axis load cell is basically a three spoke structure. Strain gauges are conveniently located on highly stressed areas. The sensing structural element is constrained to the frame of the load cell by means of special joints conceived to avoid friction. The mechanical behaviour of the load cell is described by means of analytical equations that allow a quick preliminary design focused on the given technical specifications. A finite element model has been used to asses the mechanical behaviour of the load cell.

Keywords Six-axis load cell · Sliding spherical joint · Analytical modelling · Calibration

Notation

$\boldsymbol{F}$	vector of forces and moments acting at the load cell centre
$\boldsymbol{E_b}$	vector of the strains $\varepsilon_{i\,(1=1,\ldots,6)}$
$\boldsymbol{C_b}$	load cell calibration matrix
$\boldsymbol{T}$	vector of reaction forces at the three joints N_i, $T_{i(i=1,2,3)}$
$\boldsymbol{\Delta V}$	vector of the output voltages $\Delta V_{i(i=1,\cdots,6)}$ at the Wheatstone bridges
K	gauge factor
V	excitation voltage at the Wheatstone bridges
L	spoke length
$\boldsymbol{M_i}$	calibration matrix
$\boldsymbol{M_{tst}}$	calibration matrix (statically determined structure)
$\boldsymbol{M_e}$	experimental calibration matrix
$\boldsymbol{M_{thp}}$	calibration matrix (quasi-statically determined structure)
k_a	joint axial stiffness
k_{rx}/k_{ry}	joint radial stiffnesses
k_t	joint torsional stiffness
k_{bt}/k_b	joint bending stiffnesses
$k_x/k_y/k_z$	load cell interface stiffnesses
$\boldsymbol{S}$	vector of the internal forces and moments acting at the spoke tips
$\boldsymbol{\delta_i}$	displacements and rotations at a spoke tip
$\boldsymbol{R_t}(\alpha)$	rotation matrix
$A(\omega)$	Inertance—transfer function acceleration/force
h	distance between a strain gauge and the spoke tip (see Fig. 4)
h_z	distance between a strain gauge and the three spoke structure centre (see Fig. 4)
$\boldsymbol{\nu}$	vector of the bending moments acting on the six strain gauge bridges
$\boldsymbol{\nu_{tst}}$	vector of the bending moments—statically determined structure
$\boldsymbol{\nu_{thp}}$	vector of the bending moments—quasi-statically determined structure
χ	load cell sensitivity matrix
χ_{tst}	statically determined structure sensitivity matrix
χ_{trj}	rigid joints model sensitivity matrix
χ_{trs}	rigid spokes model sensitivity matrix
$\boldsymbol{\delta\nu}$	error on the strain (bending) measurements
$\boldsymbol{\delta\chi}$	error on the sensitivity matrix

Note: bold symbol refers to a vector or a matrix

G. Mastinu · M. Gobbi (✉) · G. Previati
Department of Mechanical Engineering,
Politecnico di Milano,
Via La Masa, 1,
20156 Milan, Italy
e-mail: massimiliano.gobbi@polimi.it

Published online: 13 May 2010

Introduction

In experimental testing activities the use of multi axis load cells is widespread, e. g. balances for wind tunnels [1–4], structures [5–19],.... Many commercially available load cells are able to measure the steady or dynamic forces and moments acting on a structure [1, 5–10, 12–25]. Generally such measuring devices are quite expensive and their usage is restricted to advanced research and development activities [1, 3, 4]. The high cost is often due to the relatively complex hardware, to time consuming calibration, and to special materials used for the manufacturing.

The new six-axis load cell presented in this paper is a relatively simple device, and is basically an analog device able to measure the three components of a force and the three components of a moment acting on the load cell itself.

With respect to other similar six-axis load cells, the sensing element of the six-axis load cell is—in principle—a statically determined structure (actually, as it will be explained later, it is a quasi-statically determined structure). Such a sensing element is shaped as a three spoke structure, constrained to the external body of the load cell (frame) by means of three special joints positioned at the tip of each spoke. A proper design of the joints has been conceived in order to make friction vanish. Patents are pending on the load cell [25–28].

The six-axis load cell was especially developed for the indoor characterisation of vehicle suspension systems; see [29] for further details. The construction principle of the presented new six axis load cell has been used extensively referring to measuring hubs (a special class of six-axis load cells used to measure the forces and moments acting on a wheel [11, 25–28, 30–37]).

In the following sections, the load cell concept design [25–28], the mathematical modelling, and the embodiment design will be presented. Another paper [38], companion of this one, will present the error analysis, the construction and the experimental assessment of the performance of the load cell.

Load Cell Design Concept

The sensing element of the six-axis load cell is a three spoke structure [25–28], Fig. 1. The three spoke structure, is constrained to the outer (frame) of the load cell by means of three special joints positioned at the tip of each spoke. Each joint allows 4 degrees of freedom, i.e. three rotations and a translation (sliding) along the axis of the spoke. Such a joint will be named hereafter ‘sliding spherical joint’. The three spoke structure constrained by this type of joints (1, 2, 3 in Fig. 1) is statically determined. The proof can be obtained simply by inspection of Fig. 1, in which the two constraints (for ex. 1, 3) at two adjacent spokes are

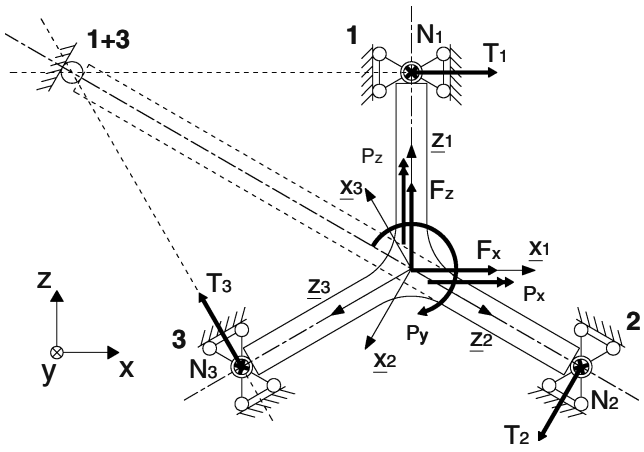

Fig. 1 Concept design of the six-axis load cell suitable to measure the 3 forces (F_x, F_y, F_z) and 3 moments (P_x, P_y, P_z) acting at the centre of the load cell. The concept design refers to a statically determined structure

equivalent to the virtual rotational joint (1+3). This virtual joint makes the structure a simply supported beam which is clearly a statically determined structure. The exploitation of a statically determined structure prevents the negative effects due to the non-uniform distribution of the temperature on the load cell and the negative effects due to the compliance of constraints.

When the load cell is loaded, the three spoke structure in Fig. 1 is subject to two forces at each spoke tip, a total of 6 forces are acting at the three spoke tips. Namely, there are the three forces T_1 T_2 T_3 and other three forces N_1 N_2 N_3 normal to them. By sensing the bending moments at each spoke root (or acting at a known position along the spokes) the six forces T_i N_i at the spoke tips are obtained. Given such six forces, the three forces and the three moments acting at the centre of the load cell ($\boldsymbol{F}$) can be computed by solving the equilibrium equations (see next Sect. Mathematical Model).

A special design [25, 28] of the sliding spherical joints has been performed in order to make friction vanish. After a comprehensive analysis, the sliding spherical joint at the spoke tip has been designed as a circular spoked structure (Fig. 2) (this circular spoked structure has not to be confused with the other three-spoke sensing structure). Some stiffnesses have been associated to the degrees of freedom of the sliding spherical joint, so actually we have an elastic sliding spherical joint. By employing these elastic joints, the whole load cell structure is no longer statically determined. Anyway, it can be considered quasi-statically determined as the three sliding spherical joints are actually springs with weak stiffness associated to the three rotations and to the sliding motion along the axis of the spoke. Figure 2 shows the geometry of the developed elastic sliding spherical joint. The central hole is fitted and fixed to each spoke tip while the outer ring is constrained to the load cell frame.

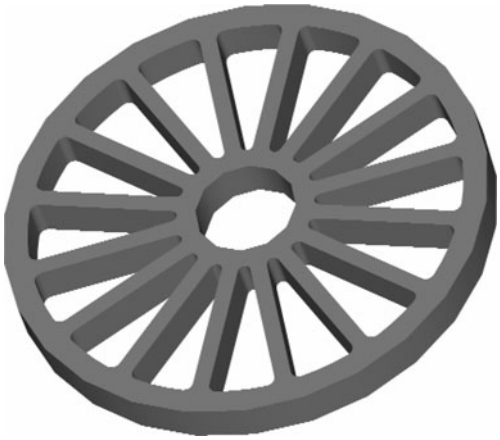

Fig. 2 Circular spoked (steel) structure as an elastic spherical sliding joint

As the target is a quasi-statically determined structure, the design of the joint stiffnesses is a fundamental task. The spoked structure in Fig. 2 has low axial, low torsional and low bending stiffness compared to radial stiffness. The design of the circular spoked structure (elastic sliding spherical joint) has been successfully performed based on analytical modelling (see Sect. Mathematical Model, the same model can be applied to design the elastic sliding spherical joint) and on finite element analysis (Fig. 3). The axial stiffness (associated to the sliding motion) is set less than 1% of the radial stiffness.

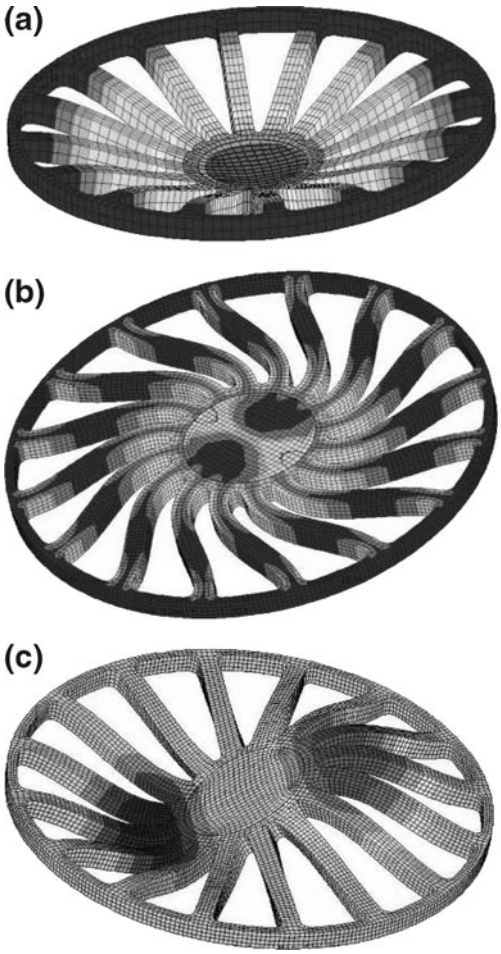

Fig. 3 FEM analysis of the elastic sliding spherical joint. Axial (**a**), torsional (**b**) and bending (**c**) deformations related to the axial, torsional and bending stiffnesses respectively

Load Cell Modeling

Mathematical Model

In this section the mechanical and mathematical modelling of the six-axis load cell is presented. Three models have been derived and used. At first, a simple model, representing the statically determined structure (shown in Fig. 1), is introduced. Then, a more refined analytical model referring to the quasi-statically determined structure, is derived which takes into account the actual stiffnesses of the elastic sliding spherical joints (Fig. 3) and the compliance of the three spokes pertaining to the sensing structure in (Fig. 4). Finally a finite element model is presented.

Let us consider:

- the vector of the forces and of the moments acting at the load cell $\mathbf{F} = [F_x \;\; F_y \;\; F_z \;\; F_x \;\; F_y \;\; F_z]$ (see coordinate system in Fig. 1),
- the vector of the strains measured at the locations shown in Fig. 4 $\mathbf{E}_s = [\varepsilon_{1a} \; \varepsilon_{1b} \; \varepsilon_{2a} \; \varepsilon_{2b} \; \varepsilon_{3a} \; \varepsilon_{3b} \; \varepsilon_{4a} \; \varepsilon_{4b} \; \varepsilon_{5a} \; \varepsilon_{5b} \; \varepsilon_{6a} \; \varepsilon_{6b}]^T$.

The following relationship holds

$$\mathbf{F} = \mathbf{F}(\mathbf{E}_s) \tag{1}$$

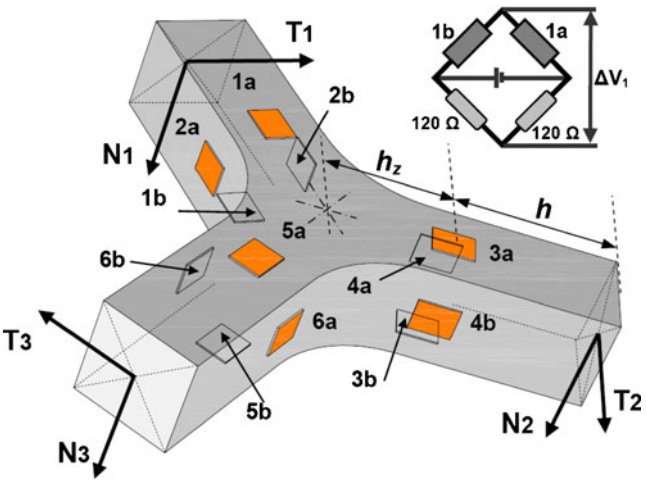

Fig. 4 Location of the 12 strain gauges

The above equation becomes $\boldsymbol{F} = \boldsymbol{C} \cdot \mathbf{E}_S$ if a linear relationship between $\boldsymbol{F}$ and $\mathbf{E}_S$ holds. As stated in the previous section, half bridge connections of the strain gauges have been used for measuring the two bending moments. Therefore the vector of the bending strains signals reduces to $\mathbf{E_b} = [\varepsilon_1 \quad \varepsilon_2 \quad \varepsilon_3 \quad \varepsilon_4 \quad \varepsilon_5 \quad \varepsilon_6]^T$. The relationship between $\boldsymbol{F}$ and $\mathbf{E_b}$ becomes:

$$\boldsymbol{F} = \boldsymbol{C_b} \cdot \mathbf{E_b} \tag{2}$$

where $\boldsymbol{C_b}$ is a 6×6 constant square matrix referred to as the load cell stiffness matrix.

By considering the ideal statically determined structure (Fig. 1), the vector $\mathbf{E_b}$ is directly related to the vector of the 6 reaction forces at the three joints $\boldsymbol{T} = [N_1 \ T_1 \ N_2 \ T_2 \ N_3 \ T_3]^T$ (Fig. 1) (l denotes the length of a single spoke)

$$\begin{bmatrix} N_1 \\ T_1 \\ N_2 \\ T_2 \\ N_3 \\ T_3 \end{bmatrix} = \begin{bmatrix} 0 & -1/3 & 0 & 2/3l & 0 & 0 \\ -2/3 & 0 & 0 & 0 & -1/3l & 0 \\ 0 & -1/3 & 0 & -1/3l & 0 & -1/l\sqrt{3} \\ 1/3 & 0 & 1/\sqrt{3} & 0 & -1/3l & 0 \\ 0 & -1/3 & 0 & -1/3l & 0 & 1/l\sqrt{3} \\ 1/3 & 0 & -1/\sqrt{3} & 0 & -1/3l & 0 \end{bmatrix} \cdot \begin{bmatrix} F_x \\ F_y \\ F_z \\ P_x \\ P_y \\ P_z \end{bmatrix} = \boldsymbol{A_{st}} \cdot \boldsymbol{F} \tag{3}$$

From the vector of the reaction forces, the strains can be derived by the following equation

$$\boldsymbol{E}_b = \frac{h}{E} \begin{bmatrix} 1/W_{xx} & 0 & 0 & 0 & 0 & 0 \\ 0 & 1/W_{yy} & 0 & 0 & 0 & 0 \\ 0 & 0 & 1/W_{xx} & 0 & 0 & 0 \\ 0 & 0 & 0 & 1/W_{yy} & 0 & 0 \\ 0 & 0 & 0 & 0 & 1/W_{xx} & 0 \\ 0 & 0 & 0 & 0 & 0 & 1/W_{yy} \end{bmatrix} \boldsymbol{T} \tag{4}$$

where E is the elastic modulus of the material, h the application arm (see Fig. 4) and W the spoke section modulus. A well-known relationship between the vector of the bridges output voltages $\boldsymbol{\Delta V}$ and the vector $\mathbf{E_b}$ exists (k and V are respectively the gauge factor and the bridge excitation voltage)

$$\Delta \boldsymbol{V} = [\Delta V_1 \Delta V_2 \Delta V_3 \Delta V_4 \Delta V_5 \Delta V_6]^T = \frac{V}{2} k \cdot \boldsymbol{E_b} \tag{5}$$

The theoretical calibration matrix $\boldsymbol{M_{tst}}$ is computed as follows

$$\begin{aligned} &\Delta \boldsymbol{V} = \left[\tfrac{V}{2} k \cdot \boldsymbol{E_b} \cdot \boldsymbol{A_{st}}\right] \cdot \boldsymbol{F} = inv(\boldsymbol{M_{tst}}) \cdot \boldsymbol{F} \\ &\boldsymbol{F} = \boldsymbol{M_{tst}} \cdot \Delta \boldsymbol{V} \end{aligned} \tag{6}$$

For square section spokes, the matrix $\boldsymbol{E_b}$ can be replaced by the scalar expression h/EW. In general, the matrix $\mathbf{M_{tst}}$ has the expression

$$M_{tst} = \frac{2}{V} \frac{1}{k} \frac{E}{h} \cdot \begin{bmatrix} 0 & 0 & 0 & \frac{3W_{yy}}{2} & 0 & \frac{3W_{yy}}{2} \\ W_{xx} & 0 & W_{xx} & 0 & W_{xx} & 0 \\ 0 & \sqrt{3}W_{yy} & 0 & \frac{\sqrt{3}W_{yy}}{2} & 0 & \frac{\sqrt{3}W_{yy}}{2} \\ -W_{xx}L & 0 & \frac{W_{xx}L}{2} & 0 & \frac{W_{xx}L}{2} & 0 \\ 0 & -3LW_{yy} & 0 & -3LW_{yy} & 0 & -3LW_{yy} \\ 0 & 0 & \frac{\sqrt{3}LW_{xx}}{2} & 0 & \frac{-\sqrt{3}LW_{xx}}{2} & 0 \end{bmatrix}$$

The actual load cell has elastic sliding spherical joints at the spoke tips (Figs. 3, 8 and 9), so, in order to compute the calibration matrix, the analytical mathematical model of the quasi-statically determined structure of the load cell has been derived. A single spoke tip pertaining to the sensing structure in Fig. 4 is shown Fig. 5. The actual stiffnesses at the spoke tip (axial 'k_a', radial 'k_{rx}–k_{ry}', torsional 'k_t' and bending 'k_{bt}–k_b' stiffnesses) are taken into account. The model accounts for the compliance of each spoke of the sensing structure, as shown in Fig. 6.

By considering

- the vector $\boldsymbol{S}$ of the 18 internal forces and moments acting at the 3 spoke at the central node of the three spoke sensing structure as shown in Fig. 5 (local coordinate system $\underline{x_i}, \underline{y_i}, \underline{z_{i(i=1,2,3)}}$ in Fig. 1),

$$\boldsymbol{S_{i(i=1,2,3)}} = \left[S_{\underline{x_i}} S_{\underline{y_i}} S_{\underline{z_i}} M_{\underline{x_i}} M_{\underline{y_i}} M_{\underline{z_i}} \right]$$

$$\boldsymbol{S} = [S_1 S_2 S_3]^T$$

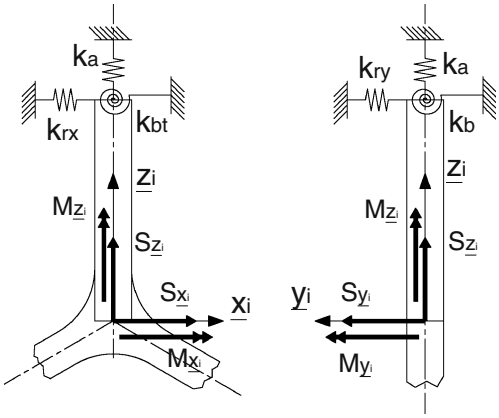

Fig. 5 Model of the six-axis load cell (quasi-statically determined structure)—only a single spoke of the sensing structure in Figs. 1 and in 4 is shown

– the 3 vectors $\boldsymbol{\delta_i}$ of the displacements "δ" and rotations "φ" of each spoke tip root (local coordinate system)

$$\boldsymbol{\delta_{i(i=1,2,3)}} = \left[\delta_{\underline{x}_i} \quad \delta_{\underline{y}_i} \quad \delta_{\underline{z}_i} \quad \varphi_{\underline{x}_i} \quad \varphi_{\underline{y}_i} \quad \varphi_{\underline{z}_i}\right]^T$$

– the rotation matrix $R_t(\alpha)(\alpha = \pm 2/3\pi)$ defined as follows

$$\boldsymbol{R_t}(\alpha) = \begin{bmatrix} \boldsymbol{R}(\alpha) & 0 \\ 0 & \boldsymbol{R}(\alpha) \end{bmatrix}$$

$$\boldsymbol{R}(\alpha) = \begin{bmatrix} \cos(\alpha) & 0 & \sin(\alpha) \\ 0 & 1 & 0 \\ -\sin(\alpha) & 0 & \cos(\alpha) \end{bmatrix}$$

In order to compute the 18 components of the vector $\boldsymbol{S}$, a 18 equations system has been written in the following form

$$\begin{cases} \boldsymbol{F} = \boldsymbol{I} \cdot \boldsymbol{S}_1 + \boldsymbol{R_t}(2/3\pi) \cdot \boldsymbol{S}_2 + \boldsymbol{R_t}(-2/3\pi) \cdot \boldsymbol{S}_3 \\ \boldsymbol{\delta}_1 = \boldsymbol{R_t}(2/3\pi) \cdot \boldsymbol{\delta}_2 \\ \boldsymbol{\delta}_1 = \boldsymbol{R_t}(-2/3\pi) \cdot \boldsymbol{\delta}_3 \end{cases} \tag{7}$$

The first equation refers to the force equilibrium at the central node (roots of the three spokes), while the other 2 equations refer to the displacement consistency at the central node between the spokes 1–2 and 1–3 respectively. The displacements and rotations of each spoke are computed as follows. Figure 6 shows the displacement of a spoke root in the $\underline{x}$ local direction when a force $-\mathrm{S}_{\underline{x}}$ acts.

The total displacement $\delta_{\underline{x}}(\mathrm{S}_{\underline{x}})$ depends on the radial and bending compliances of the elastic sliding spherical joint (respectively $\delta_{\underline{x}}(k_{rx})$ and $\delta_{\underline{x}}(k_{bt})$), additionally $\delta_{\underline{x}}(\mathrm{S}_{\underline{x}})$ depends on the compliance of the spoke $(\delta_{\underline{x}}(J_y))$

$$\delta_{\underline{x}}(S_{\underline{x}}) = d_{\underline{x}}(k_{rx}) + d_{\underline{x}}(J_y) + d_{\underline{x}}(k_{bt})$$

$$\delta_{\underline{x}}(S_{\underline{x}}) = \frac{S_{\underline{x}}}{k_{rx}} + \frac{S_{\underline{x}} l^3}{3EJ_y} + \frac{S_{\underline{x}} l^2}{k_{bt}} \tag{8}$$

The force $S_{\underline{x}}$ produces a rotation of the spoke tip around the $\underline{y}$ local axis, due to the bending compliance of the sliding spherical joint (k_{bt}) and due to the spoke bending compliance respectively

$$\varphi_{\underline{y}}(S_{\underline{x}}) = -\frac{S_{\underline{x}} l}{k_{bt}} - \frac{S_{\underline{x}} l^2}{2EJ_y} \tag{9}$$

A similar approach has been followed to derive all the displacements and rotations resulting at each spoke root ($S_{\underline{x}} \rightarrow \delta_{\underline{x}}(S_{\underline{x}})/\varphi_{\underline{y}}(S_{\underline{x}}), S_{\underline{y}} \rightarrow \delta_{\underline{y}}(S_{\underline{y}})/\varphi_{\underline{x}}(S_{\underline{y}}), S_{\underline{z}} \rightarrow \delta_{\underline{z}}(S_{\underline{z}}), M_{\underline{x}} \rightarrow \delta_{\underline{y}}(M_{\underline{x}})/\varphi_{\underline{x}}(M_{\underline{x}}), M_{\underline{y}} \rightarrow \delta_{\underline{x}}(M_{\underline{y}})/\varphi_{\underline{y}}(M_{\underline{y}}), M_{\underline{z}} \rightarrow \varphi_{\underline{z}}(M_{\underline{z}})$ see equation (10)). All the parameters pertaining to each of the three spokes (e.g. l, J_y,...) are assumed to be equal. The following relationship between the vector of the displacements and rotations $\boldsymbol{\delta_i}$ (at the spoke root)

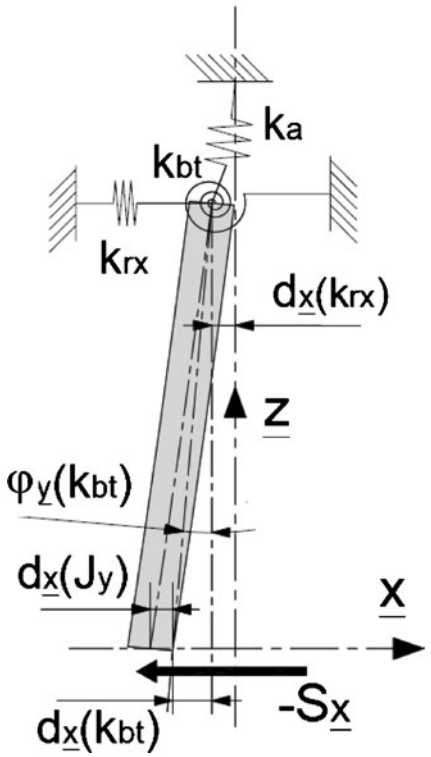

Fig. 6 The displacement in the $\underline{x}$ direction of a spoke root, due to a force $-S_{\underline{x}}$

and the vector of the internal forces and moments $\boldsymbol{S_i}$ holds $\boldsymbol{\delta_i} = \Delta \cdot \boldsymbol{S_i}$, where

$$\Delta = \begin{bmatrix} \frac{1}{k_{rx}} + \frac{l^3}{3EJ_y} + \frac{l^2}{k_{bt}} & 0 & 0 & 0 & -\frac{l^2}{2EJ_y} - \frac{l}{k_{bt}} & 0 \\ 0 & \frac{1}{k_{ry}} + \frac{l^3}{3EJ_x} + \frac{l^2}{k_b} & 0 & \frac{l^2}{2EJ_x} + \frac{l}{k_b} & 0 & 0 \\ 0 & 0 & \frac{1}{k_a} + \frac{l}{EA} & 0 & 0 & 0 \\ 0 & \frac{l}{k_b} + \frac{l^2}{2EJ_x} & 0 & \frac{1}{k_b} + \frac{l}{EJ_x} & 0 & 0 \\ -\frac{l}{k_{bt}} - \frac{l^2}{2EJ_y} & 0 & 0 & 0 & \frac{1}{k_{bt}} + \frac{l}{EJ_y} & 0 \\ 0 & 0 & 0 & 0 & 0 & \frac{1}{k_t} + \frac{l}{GJ_p} \end{bmatrix} \tag{10}$$

Where J_P accounts for the torsion cross section coefficient of non circular sections. The system in equation (7) can be rewritten in the following compact form

$$\begin{bmatrix} \boldsymbol{I} & \boldsymbol{R_t}(2/3\pi) & \boldsymbol{R_t}(-2/3\pi) \\ \Delta & -\boldsymbol{R_t}(2/3\pi) \cdot \Delta & 0 \\ \Delta & 0 & -\boldsymbol{R_t}(-2/3\pi) \cdot \Delta \end{bmatrix} \cdot \boldsymbol{S} = \begin{bmatrix} \boldsymbol{F} \\ 0 \\ 0 \end{bmatrix} \tag{11}$$

The above system has been solved symbolically, the 18 components of internal forces and moments $\boldsymbol{S}$, have been found as function of the vector $\boldsymbol{F}$ of force and moment acting at the load cell.

$$\boldsymbol{S} = \boldsymbol{S}(\boldsymbol{F})$$

The above system equation reads

$$\begin{aligned} &S_{\underline{x}_1}, M_{\underline{y}_1} = f\left(F_x, T_y\right) \\ &S_{\underline{y}_1}, M_{x_1} = f\left(F_y, T_x\right) \\ &S_{\underline{x}_{2-3}}, M_{\underline{y}_{2-3}} = f\left(F_x, F_z, T_y\right) \\ &S_{\underline{y}_{2-3}}, M_{\underline{x}_{2-3}} = f\left(F_y, T_x, T_z\right) \\ &S_{\underline{z}_1} = f(F_z); M_{\underline{z}_1} = f(T_z) \\ &S_{\underline{z}_{2-3}} = f(F_x, F_z) \\ &M_{\underline{z}_{2-3}} = f(T_x, T_z) \end{aligned} \tag{12}$$

The analytical expressions of equation system (12) are reported in Appendix.

As the vector of the internal forces and moments $\boldsymbol{S}$ has been computed, it is possible to compute the output differential voltages $\boldsymbol{\Delta V}$ of the Wheatstone bridges (see (5)). Let us consider the single spoke shown in Fig. 10. The output voltage (strain gauges $\mathrm{iA} - \mathrm{iB}_{(\mathrm{i}=1,..,6)}$, corresponding strains $\varepsilon_{\mathrm{iA}} - \varepsilon_{\mathrm{iB(i}=1,..,6)}$ respectively) can be computed by the following equation

$$\Delta V_i = \frac{V}{4} k(\varepsilon_{iA} - \varepsilon_{iB}) \tag{13}$$

The voltages are function of the system parameters (joint stiffnesses, three spoke structure geometry, strain gauges characteristics,...) and of the vector $\boldsymbol{F}$ of the force and of the moment acting at the load cell centre

$$\Delta V_i = \Delta V_i(\boldsymbol{S}) = [\boldsymbol{M}_{\Delta V_i}]\boldsymbol{F}$$

$$\Delta \boldsymbol{V} = \begin{bmatrix} M_{\Delta V_1} \\ M_{\Delta V_2} \\ M_{\Delta V_3} \\ M_{\Delta V_4} \\ M_{\Delta V_5} \\ M_{\Delta V_6} \end{bmatrix} \cdot \boldsymbol{F} \tag{14}$$

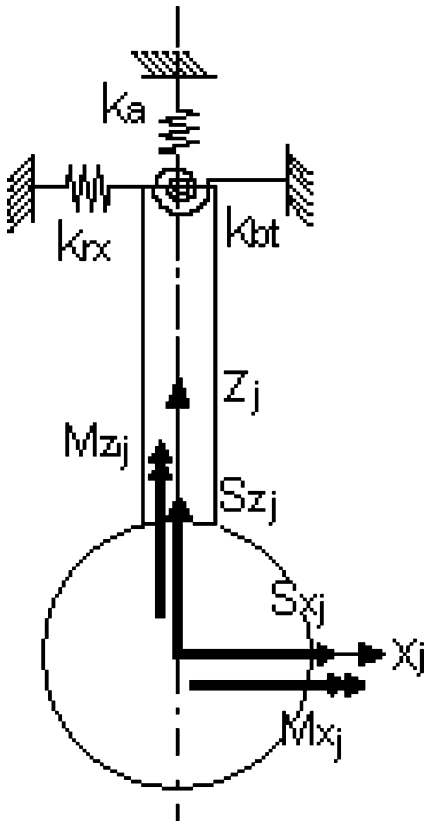

Fig. 7 One spoke of the load cell model with rigid ring

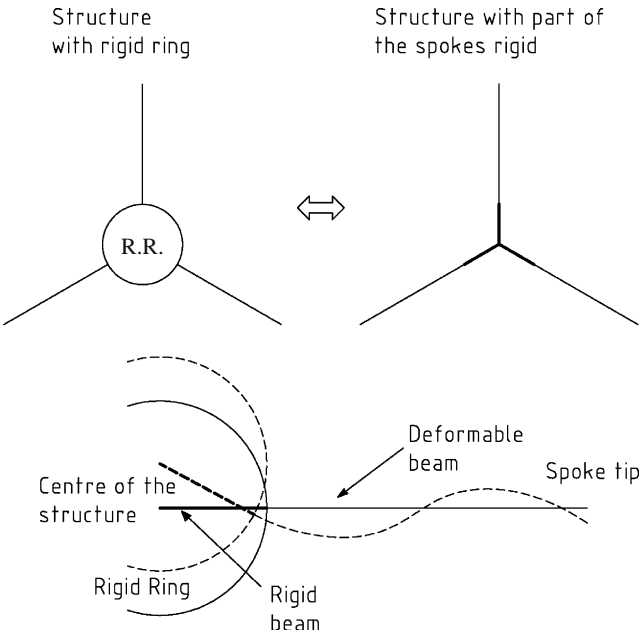

Fig. 8 Structure with central rigid ring (R.R.). *Bold line* rigid parts of the spokes. *Continuous line* non-deformed structure. *Dotted line* Qualitatively deformation of the spoke

By simply inverting the terms in equation (14), the calibration matrix $\boldsymbol{M_{thp}}$ can be derived:

$$\Delta \boldsymbol{V} = \hat{\boldsymbol{M}} \cdot \boldsymbol{F} \Rightarrow \boldsymbol{F} = \boldsymbol{M_{thp}} \cdot \Delta \boldsymbol{V} \tag{15}$$

The three spokes are connected to the central part of the structure (see Figs. 5 and 7). The central part of the three spoke structure has a very low compliance and it can be considered rigid with respect to the spokes. The very low compliance of this component of the structure can be taken into account as follows:

- a rigid ring is considered to model the central part of the structure (Fig. 7)
- the three beams representing the spokes of the structure are connected to the rigid ring
- the rigid ring is modelled as a rigid beam connecting each spoke to the centre of structure. Thus each spoke is composed by a deformable and by a non-deformable part.
- the deformable length of each spoke is calculated as the difference between the spoke length (l) and the radius of the rigid disk (r)
- the equations referring to the displacement consistency of the structure have been modified to include the rigid part of each spoke.

The described procedure is depicted in Fig. 8. The resulting system has been solved symbolically and the expression of the internal forces and moments **S** have been reported in Appendix.

Load Cell Construction

Load Cell Technical Specifications

The technical specifications of the six-axis load cell were derived in order to perform experimental tests on a vehicle suspension system [11]. The design forces and moments are respectively (Fig. 1):

– 10 kN (F_y along load cell axis), 5 kN (F_x, F_z)
– 0.5 kNm (P_x, P_y, P_z)

Additionally, the first natural frequency of the load cell has to be over 500 Hz in order to perform high frequency measurement of the forces acting on the suspension system under test. The natural frequency has been computed by considering the load cell constrained as in an experimental test. That is, the load cell is connected to a very siff surface

Table 1 Comparison between the analytical model and the corresponding FEM model

Half bridge n°	Load case								
	Fy [1000 N]			*Px* [1000 Nm]			*Pz* [1000 Nm]		
	Analytical model	FEM model	Difference %	Analytical model	FEM model	Difference %	Analytical model	FEM model	Difference %
1	42.9	44.4	3.25	2172	2166	0.25	–	–	–
3	42.9	44.4	3.25	−1086	−1083	0.25	−1881	−1876	0.25
5	42.9	44.4	3.25	−1086	−1083	0.25	1881	1876	0.25
Half bridge n°	Load case								
	Fx [1000 N]			*Fz* [1000 N]			*Py* [1000 Nm]		
	Analytical model	FEM model	Difference %	Analytical model	FEM model	Difference %	Analytical model	FEM model	Difference %
2	79.5	76.1	4.45	–	–	–	1103	1132	2.65
4	−39.8	−38.1	4.45	−68.8	−65.9	4.45	1103	1132	2.65
6	−39.8	−38.1	4.45	68.8	65.9	4.45	1103	1132	2.65

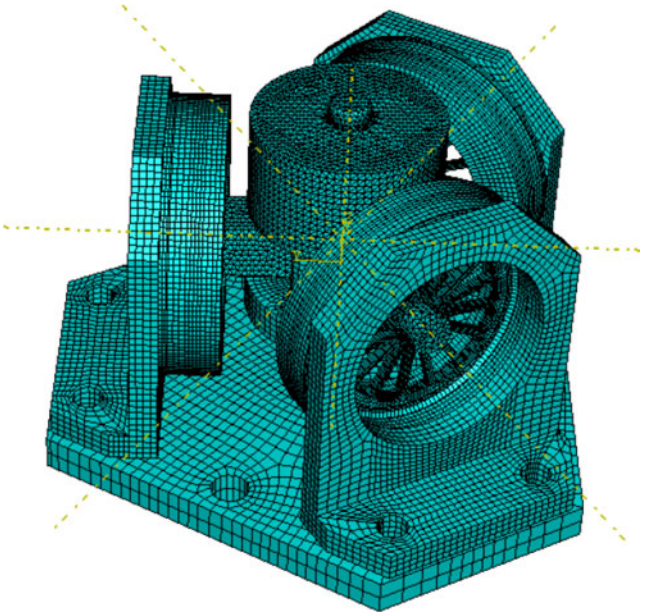

Fig. 9 FEM model of the load cell

by means of the three connecting holes on the base of the load cell (see Fig. 10).

FEM Model of the Load Cell

Given F_x, F_y, F_z, P_x, P_y, P_z the reaction forces at the joints can be computed by equation (3). Thus a preliminary design of both the joints and the three spoke structure can be performed. On the basis of the preliminary design, a FEM model of the load cell has been realized. The FEM model (Fig. 8) takes into account all the mechanical components needed to realize the load cell.

This FEM model has been used to optimize the design in terms of mechanical strength and stiffness of the components. The sensing structure has been optimized in order to get the maximum level of stress in the zones of application of the strain gauges.

The comparison between the analytical model of the load cell and the corresponding FEM model is reported in Table 1. The comparison shows the values of the deformations read by the half bridges on each spoke. The half bridges are numbered as shown in Fig. 4. The computations have been performed for the six pure loads (three forces and three moments, see Fig. 1 for symbols). Being that the system is linear, any other load case is a linear combination of the considered load cases. The table is divided into two parts. In the first part the odd half bridges are considered. These half bridges read only the deformation due to *Fy*, *Px* and *Pz*. In the second part the even half bridges. These half bridges read only the deformation due to *Fx*, *Fz* and *Py*. The comparison shows a satisfying agreement between the two models.

Embodiment Design

The drawing of the prototype six-axis load cell is shown in Fig. 9.

Particular attention has been devoted in designing the reference vertical axis of the load cell, defined by pins (see Fig. 10). The sliding spherical joint (Figs. 2 and 3) has been constrained to the load cell structure by means of ring nuts. Each spoke has been connected to the corresponding sliding spherical joint by means of a nut which compresses the annular inner part of the corresponding sliding spherical joint and realizes the constraint.

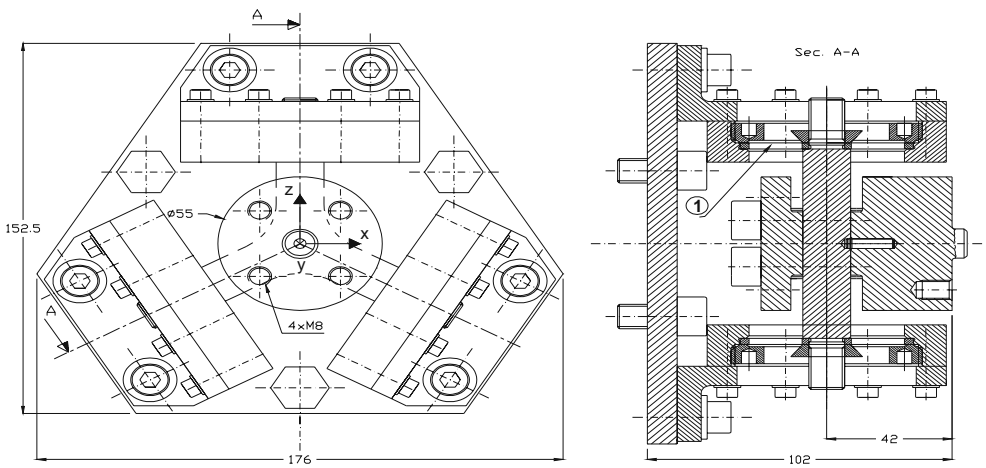

Fig. 10 Mechanical drawing of the six-axis load cell (dimensions are in *mm*)

A flange provided with 4 threaded holes aligned along the x and z load cell axes is the connection interface with the tested structure. The forces and moments measured by the load cell refer to the centre of the cell (i.e. centre of the three spoke structure).

The overall dimensions of the assembled load cell are about 150 × 175 × 100 mm. The mass is about 5 kg.

The embodiment design considered the sequence that is needed for assembling the load cell. Such sequence is crucial for aligning the vertical axis to the centre line of the load cell and for suppressing internal pre-loads, dangerous for structural integrity.

Conclusions

This paper has been devoted to the design of a new six axis load cell. The sensing element of the load cell is a quasi-statically determined three spoke structure constrained by means of elastic sliding spherical joints. The design of such joints has been performed in order to avoid friction. Twelve resistive strain gauges have been used to measure bending deformations at the three spokes of the sensing structure. The vector of the external forces and moments applied at the load cell is linearly related to six voltage output signals via a square calibration matrix. Different mathematical models have been derived to design the load cell and to tune its performances. Particular attention has been devoted to the derivation of an analytical model of the quasi-statically determined structure of the load cell. This has enabled the preliminary design of the load cell. A finite element model has been derived to assess the stress-strain behaviour of the load cell. A comparison between the analytical model and the finite element model has been performed with satisfactory results. The six axis load cell is relatively simple to be manufactured and the embodiment design has been presented. The error analysis, the construction and the experimental assessment of the performances of the load cell are presented in another paper, which is the companion paper of this one.

Appendix

Analytical expressions of the 18 internal forces and moments acting at the 3 spoke tips (rigid disk considered in the model):

$$S_{\underline{x}_1}$$

$$\left(\begin{array}{l} -1/3\left(1/3\frac{L^3}{EJy}+\frac{RL(R+L)}{EJy}+krx^{-1}+\frac{(R+L)^2}{kbt}\right)\left(\frac{L}{EJy}+kbt^{-1}\right)Ty\left(-1/2\frac{L^2}{EJy}-\frac{RL}{EJy}+\frac{-R-L}{kbt}\right) \\ +2/3Fx\left(1/3\frac{L^3}{EJy}+\frac{RL(R+L)}{EJy}+krx^{-1}+\frac{(R+L)^2}{kbt}\right)\left(\frac{L}{EJy}+kbt^{-1}\right) \\ \cdot\left(\frac{L}{EA}+ka^{-1}\right)+1/3\left(-1/2\frac{L^2}{EJy}-\frac{RL}{EJy}+\frac{-R-L}{kbt}\right)^3 Ty-1/3\left(-1/2\frac{L^2}{EJy}-\frac{RL}{EJy}+\frac{-R-L}{kbt}\right)\left(\frac{L}{EJy}+kbt^{-1}\right)Ty\left(\frac{L}{EA}+ka^{-1}\right) \end{array} \right)$$

$$\left(-\left(-1/2\frac{L^2}{EJy}-\frac{RL}{EJy}+\frac{-R-L}{kbt}\right)^2+\left(1/3\frac{L^3}{EJy}+\frac{RL(R+L)}{EJy}+krx^{-1}+\frac{(R+l)^2}{kbt}\right)\left(\frac{L}{EJy}+kbt^{-1}\right)+\left(\frac{L}{EJy}+kbt^{-1}\right)\left(\frac{L}{EA}+ka^{-1}\right)\right)^{-1}$$

$$\left(1/3\frac{L^3}{EJy}+\frac{RL(R+L)}{EJy}+krx^{-1}+\frac{(R+L)^2}{kbt}\right)^{-1}$$

$$S_{y_1}$$

$$\left(\begin{array}{l} 1/3\left(-\frac{L^2}{EJx}-2\frac{RL}{EJx}-2\frac{R+L}{kb}\right)Tx\left(\frac{L}{JpG}+kt^{-1}\right)-1/3Fy\left(1/2\frac{L^2}{EJx}+\frac{RL}{EJx}+\frac{R+L}{kb}\right)^2 \\ \quad +1/3\left(1/3\frac{L^3}{EJx}+\frac{RL(R+L)}{EJx}+kry^{-1}+\frac{(R+L)^2}{kb}\right)Fy\left(\frac{L}{JpG}+Kt^{-1}\right) \\ \quad +1/3\left(\frac{L}{EJx}+kb^{-1}\right)\left(1/3\frac{L^3}{EJx}+\frac{RL(R+L)}{EJx}+kry^{-1}+\frac{(R+L)^2}{kb}\right)Fy \end{array}\right)$$

$$\left(\begin{array}{l} \left(1/3\frac{L^3}{EJx}+\frac{RL(R+L)}{EJx}+kry^{-1}+\frac{(R+L)^2}{kb}\right)\left(\frac{L}{JpG}+kt^{-1}\right)+\left(\frac{L}{EJx}+kb^{-1}\right)\cdot \\ \left(1/3\frac{L^3}{EJx}+\frac{RL(R+L)}{EJx}+kry^{-1}+\frac{(R+L)^2}{kb}\right)-\left(1/2\frac{L^2}{EJx}+\frac{RL}{EJx}+\frac{R+L}{kb}\right)^2 \end{array}\right)^{-1}$$

$$S_{z_1}$$

$$2/3FZ\left(-\left(-1/2\frac{L^2}{EJy}-\frac{RL}{EJy}+\frac{-R-L}{kbt}\right)^2+\left(1/3\frac{L^3}{EJy}+\frac{RL(R+L)}{EJy}+krx^{-1}+\frac{(R+L)^2}{kbt}\right)\left(\frac{L}{EJy}+kbt^{-1}\right)\right)$$
$$\left(-\left(-1/2\frac{L^2}{EJy}-\frac{RL}{EJy}+\frac{-R-L}{kbt}\right)^2+\left(1/3\frac{L^3}{EJy}+\frac{RL(R+L)}{EJy}+krx^{-1}+\frac{(R+L)^2}{kbt}\right)\left(\frac{L}{EJy}+kbt^{-1}\right)+\left(\frac{L}{EJy}+kbt^{-1}\right)+\left(\frac{L}{EA}+Ka^{-1}\right)\right)^{-1}$$

$$M_{x_1}$$

$$\left(\begin{array}{l} 2/3Tx\left(\frac{L}{JpG}+kt^{-1}\right)\left(1/3\frac{L^3}{EJx}+\frac{RL(R+L)}{EJx}+Kry^{-1}+\frac{(R+L)^2}{kb}\right)\left(\frac{L}{EJx}+Kb^{-1}\right) \\ \quad -1/3\left(1/3\frac{L^3}{EJx}+\frac{RL(R+L)}{EJx}+kry^{-1}+\frac{(R+L)^2}{kb}\right)Fy\left(\frac{L}{JpG}+kt^{-1}\right)\cdot \\ \cdot\left(1/2\frac{L^2}{EJx}+\frac{RL}{EJx}+\frac{R+L}{kb}\right)-1/3\left(\frac{L}{EJx}+kb^{-1}\right)\left(1/3\frac{L^3}{EJx}+\frac{RL(R+L)}{EJx}+kry^{-1}+\frac{(R+L)^2}{kb}\right) \\ \quad Fy\left(1/2\frac{L^2}{EJx}+\frac{RL}{EJx}+\frac{R+L}{kb}\right)+1/3Fy\left(1/2\frac{L^2}{EJx}+\frac{RL}{EJx}+\frac{R+L}{kb}\right)^3 \end{array}\right)$$

$$\cdot\left(\frac{L}{EJx}+kb^{-1}\right)^{-1}\left(\begin{array}{l} \left(1/3\frac{L^3}{EJX}+\frac{RL(R+L)}{EJX}+kry^{-1}+\frac{(R+L)^2}{kb}\right)\left(\frac{L}{JpG}+kt^{-1}\right) \\ \quad +\left(\frac{L}{EJx}+kb^{-1}\right)\left(1/3\frac{L^3}{EJx}+\frac{RL(R+L)}{EJx}+kry^{-1}+\frac{(R+L)^2}{kb}\right)-\left(1/2\frac{L^2}{EJx}+\frac{RL}{EJx}+\frac{R+L}{kb}\right)^2 \end{array}\right)^{-1}$$

$$M_{y_1}$$

$$\left(\begin{array}{l} -1/3Ty\left(-1/2\dfrac{L^2}{EJy}-\dfrac{RL}{EJy}+\dfrac{-R-L}{kbt}\right)^2+1/3\left(1/3\dfrac{L^3}{EJy}+\dfrac{RL(R+L)}{EJy}+krx^{-1}\dfrac{(R+L)^2}{kbt}\right)\left(\dfrac{L}{EJy}+kbt^{-1}\right)Ty \\ +1/3\left(\dfrac{L}{EJy}+kbt^{-1}\right)Ty\left(\dfrac{L}{EA}+ka^{-1}\right)-1/3\left(-\dfrac{L^2}{EJy}-2\dfrac{RL}{EJy}+2\dfrac{-R-L}{kbt}\right)Fx\left(\dfrac{L}{EA}+ka^{-1}\right) \end{array}\right)$$

$$\left(-\left(-1/2\frac{L^2}{EJy}-\frac{RL}{EJy}+\frac{-R-L}{kbt}\right)^2+\left(1/3\frac{L^3}{EJy}+\frac{RL(R+L)}{EJy}+krx^{-1}+\frac{(R+L)^2}{kbt}\right)\left(\frac{L}{Ejy}+kbt^{-1}\right)+\left(\frac{L}{EJy}+kbt^{-1}\right)\left(\frac{L}{EA}+ka^{-1}\right)\right)^{-1}$$

$$M_{z_1}$$

$$2/3Tz\left(\left(\frac{1}{EJx}+kb^{-1}\right)\left(1/3\frac{L^3}{EJx}+\frac{RL(R+L)}{EJx}+kry^{-1}+\frac{(R+L)^2}{kb}\right)-\left(1/2\frac{L^2}{EJx}+\frac{RL}{EJx}+\frac{R+L}{kb}\right)^2\right)$$

$$\left(\begin{array}{l} \left(1/3\dfrac{L^3}{EJx}+\dfrac{RL(R+L)}{EJx}+kry^{-1}+\dfrac{(R+L)^2}{kb}\right)\left(\dfrac{L}{JpG}+kt^{-1}\right)+ \\ \qquad +\left(\dfrac{L}{EJx}+kb^{-1}\right)\left(1/3\dfrac{L^3}{EJx}+\dfrac{RL(R+L)}{EJx}+kry^{-1}+\dfrac{(R+L)^2}{kb}\right)-\left(1/2\dfrac{L^2}{EJx}+\dfrac{RL}{EJx}+\dfrac{R+L}{kb}\right)^2 \end{array}\right)^{-1}$$

$$S_{x_2}$$

$$\left(\begin{array}{l} -1/3\left(1/3\dfrac{L^3}{EJy}+\dfrac{RL(R+L)}{EJy}+krx^{-1}+\dfrac{(R+L)^2}{kbt}\right)\sqrt{3}\left(\dfrac{L}{EJy}+kbt^{-1}\right)Fz\left(\dfrac{L}{EA}+ka^{-1}\right) \\ -1/3Fx\left(1/3\dfrac{L^3}{EJy}+\dfrac{RL(R+L)}{EJy}+krx^{-1}+\dfrac{R+L^2}{kbt}\right)\left(\dfrac{L}{EJy}+kbt^{-1}\right)\left(\dfrac{L}{EA}+ka^{-1}\right)+1/3\left(-1/2\dfrac{L^2}{EJy}-\dfrac{RL}{EJy}+\dfrac{-R-L}{kbt}\right)^3 \\ Ty-1/3\left(1/3\dfrac{L^3}{EJy}+\dfrac{RL(R+L)}{EJy}+krx^{-1}+\dfrac{(R+L)^2}{kbt}\right)\left(\dfrac{L}{EJy}+kbt^{-1}\right)Ty\left(-1/2\dfrac{L^2}{EJy}-\dfrac{RL}{EJy}+\dfrac{-R-L}{kbt}\right) \\ -1/3\left(-1/2\dfrac{L^2}{EJy}-\dfrac{RL}{EJy}+\dfrac{-R-L}{kbt}\right)\cdot\left(\dfrac{L}{EJy}+kbt^{-1}\right)Ty\left(\dfrac{L}{EA}+ka^{-1}\right) \end{array}\right)$$

$$\left(-\left(-1/2\frac{L^2}{EJy}-\frac{RL}{EJy}+\frac{-R-L}{kbt}\right)^2+\left(1/3\frac{L^3}{EJy}+\frac{RL(R+L)}{EJy}+krx^{-1}+\frac{(R+L)^2}{kbt}\right)+\left(\frac{L}{EJy}+kbt^{-1}\right)+\left(\frac{L}{EJy}+kbt^{-1}\right)\left(\frac{L}{EA}+ka^{-1}\right)\right)$$

$$\cdot\left(1/3\frac{L^3}{EJy}+\frac{RL(R+L)}{EJy}+krx^{-1}+\frac{(R+L)^2}{kbt}\right)^{-1}$$

$$S_{y_2}$$

$$\begin{pmatrix} 1/3\left(1/3\dfrac{L^3}{EJr}+\dfrac{RL(R+L)}{EJx}+kry^{-1}+\dfrac{(R+L)^2}{kb}\right)Fy\left(\dfrac{L}{JpG}+kt^{-1}\right)+1/3\left(\dfrac{L}{EJr}+kb^{-1}\right)\left(1/3\dfrac{L^3}{EJx}+\dfrac{RL(R+L)}{EJx}+kry^{-1}+\dfrac{(R+L)^2}{kb}\right) \\ Fy-1/3Fy\left(1/2\dfrac{L^2}{EJx}+\dfrac{RL}{EJx}+\dfrac{R+L}{kb}\right)^2+1/3\left(1/2\dfrac{L^2}{EJx}+\dfrac{RL}{EJx}+\dfrac{R+L}{kb}\right)Tx\left(\dfrac{L}{JpG}+kt^{-1}\right) \\ +1/3\left(1/2\dfrac{L^2}{EJx}+\dfrac{RL}{EJx}+\dfrac{R+L}{kb}\right)\sqrt{3}\left(\dfrac{L}{JpG}+kt^{-1}\right)Tz \end{pmatrix}$$

$$\begin{pmatrix} \left(1/3\dfrac{L^3}{EJx}+\dfrac{RL(R+L)}{EJx}+kry^{-1}+\dfrac{(R+L)^2}{kb}\right)\left(\dfrac{L}{JpG}+kt^{-1}\right)+\left(\dfrac{L}{EJx}+kb^{-1}\right)\left(1/3\dfrac{L^3}{EJx}+\dfrac{RL(R+L)}{EJx}+kry^{-1}+\dfrac{(R+L)^2}{kb}\right) \\ -\left(1/2\dfrac{L^2}{EJx}+\dfrac{RL}{EJx}+\dfrac{R+L}{kb}\right)^2 \end{pmatrix}^{-1}$$

$$S_{z_2}$$

$$\begin{pmatrix} 1/3\left(-1/2\dfrac{L^2}{EJy}-\dfrac{RL}{EJy}+\dfrac{-R-L}{kbt}\right)^2Fz-1/3\left(\dfrac{L}{EJy}+kbt^{-1}\right)Fz\left(1/3\dfrac{L^3}{EJy}+\dfrac{RL(R+L)}{EJy}+krz^{-1}+\dfrac{(R-L)^2}{kbt}\right) \\ -1/3\sqrt{3}\left(-1/2\dfrac{L^2}{EJy}-\dfrac{RL}{EJy}+\dfrac{-R-L}{kbt}\right)^2Fx+1/3\sqrt{3}\left(\dfrac{L}{EJy}+kbt^{-1}\right)Fx\left(1/3\dfrac{L^3}{EJy}+\dfrac{RL(R+L)}{EJy}+krz^{-1}-\dfrac{(R+L)^2}{kbt}\right) \end{pmatrix}$$

$$\left(-\left(-1/2\dfrac{L^2}{EJy}+\dfrac{RL}{EJy}+\dfrac{-R-L}{kbt}\right)^2+\left(1/3\dfrac{L^3}{EJy}+\dfrac{RL(R+L)}{EJy}+krx^{-1}+\dfrac{(R+L)^2}{kbt}\right)\left(\dfrac{L}{EJy}+kbt^{-1}\right)+\left(\dfrac{L}{EJy}+kbt^{-1}\right)\left(\dfrac{L}{EA}+ka^{-1}\right)\right)^{-1}$$

$$M_{x_2}$$

$$\begin{pmatrix} 1/3\left(\dfrac{L}{EJx}+kb^{-1}\right)\left(1/3\dfrac{L^3}{EJx}+\dfrac{RL(R+L)}{EJx}+kry^{-1}+\dfrac{(R+L)^2}{kb}\right)Fy\left(1/2\dfrac{L^2}{EJx}+\dfrac{RL}{EJx}+\dfrac{R+L}{kb}\right) \\ -1/3\sqrt{3}\left(\dfrac{L}{JpG}+kt^{-1}\right)Tz\left(\dfrac{L}{EJx}+kb^{-1}\right)\left(1/3\dfrac{L^3}{EJx}+\dfrac{RL(R+L)}{EJx}+kry^{-1}+\dfrac{(R+L)^2}{kb}\right) \\ -1/3Tx\left(\dfrac{L}{JpG}+kt^{-1}\right)\left(1/3\dfrac{L^3}{EJx}+\dfrac{RL(R+L)}{EJx}+kry^{-1}+\dfrac{(R+L)^2}{kb}\right)\left(\dfrac{L}{EJx}+kb^{-1}\right) \\ -1/3\left(1/3\dfrac{L^3}{EJx}+\dfrac{RL(R+L)}{EJx}+kry^{-1}+\dfrac{(R+L)^2}{kb}\right)Fy\left(\dfrac{L}{JpG}+kt^{-1}\right)\cdot\left(1/2\dfrac{L^2}{EJx}+\dfrac{RL}{EJx}+\dfrac{R+L}{kb}\right)+1/3Fy\left(1/2\dfrac{L^2}{EJx}+\dfrac{RL}{EJx}+\dfrac{R+L}{kb}\right)^3 \end{pmatrix}$$

$$\left(\dfrac{L}{EJx}+kb^{-1}\right)^{-1}\begin{pmatrix} \left(1/3\dfrac{L^3}{EJx}+\dfrac{RL(R+L)}{EJx}+kry^{-1}+\dfrac{(R+L)^2}{kb}\right)\left(\dfrac{L}{JpG}+kt^{-1}\right)+\left(\dfrac{L}{EJx}+kb^{-1}\right)\cdot\left(1/3\dfrac{L^3}{EJx}+\dfrac{RL(R+L)}{EJx}+kry^{-1}+\dfrac{(R+L)^2}{kb}\right) \\ -\left(1/2\dfrac{L^2}{EJx}+\dfrac{RL}{EJx}+\dfrac{R+L}{kb}\right)^2 \end{pmatrix}^{-1}$$

$$M_{y_2}$$

$$\begin{pmatrix} -1/3Ty\left(-1/2\frac{L^2}{EJy}-\frac{RL}{EJy}+\frac{-R-L}{kbt}\right)^2+1/3\left(1/3\frac{L^3}{EJy}+\frac{RL(R+L)}{EJy}+krx^{-1}+\frac{(R+L)^2}{kbt}\right)\left(\frac{L}{EJy}+kbt^{-1}\right)Ty \\ +1/3\left(\frac{L}{EJy}+kbt^{-1}\right)Ty\left(\frac{L}{EA}+ka^{-1}\right)+1/3\sqrt{3}\left(-1/2\frac{L^2}{EJy}-\frac{RL}{EJy}+-\frac{-R-L}{kbt}\right)\left(\frac{L}{EA}+ka^{-1}\right)Fz \\ +1/3\left(-1/2\frac{L^2}{EJy}-\frac{RL}{EJy}+\frac{-R-L}{kbt}\right)Fx\left(\frac{L}{EA}+ka^{-1}\right) \end{pmatrix}$$

$$\begin{pmatrix} -\left(-1/2\frac{L^2}{EJy}-\frac{RL}{EJy}+\frac{-R-L}{kbt}\right)^2+\left(1/3\frac{L^3}{EJy}+\frac{RL(R+L)}{EJy}+krx^{-1}+\frac{(R+L)^2}{kbt}\right)\cdot\left(\frac{L}{EJy}+kbt^{-1}\right) \\ +\left(\frac{L}{EJy}+kbt^{-1}\right)\left(\frac{L}{EA}+ka^{-1}\right) \end{pmatrix}^{-1}$$

$$M_{z_2}$$

$$\begin{pmatrix} -1/3\sqrt{3}\left(1/2\frac{L^2}{EJx}+\frac{RL}{EJx}+\frac{R+L}{kb}\right)^2Tx+1/3\left(1/2\frac{L^2}{EJx}+\frac{RL}{EJx}+\frac{R+L}{kb}\right)^2Tz \\ +1/3\left(\frac{L}{EJx}+kb^{-1}\right)\left(1/3\frac{L^3}{EJx}+\frac{RL(R+L)}{EJx}+kry^{-1}+\frac{(R+L)^2}{kb}\right)\sqrt{3}Tx-1/3\left(\frac{L}{EJx}+kb^{-1}\right)\cdot\left(1/3\frac{L^3}{EJx}+\frac{RL(R+L)}{EJx}+kry^{-1}+\frac{(R+L)^2}{kb}\right)Tz \end{pmatrix}$$

$$\begin{pmatrix} \left(1/3\frac{L^3}{EJx}+\frac{RL(R+L)}{EJx}+kry^{-1}+\frac{(R+L)^2}{kb}\right)\left(\frac{L}{JpG}+kt^{-1}\right)+\left(\frac{L}{EJx}+kb^{-1}\right)\left(1/3\frac{L^3}{EJx}+\frac{RL(R+L)}{EJx}+kry^{-1}+\frac{(R+L)^2}{kb}\right) \\ -\left(1/2\frac{L^2}{EJx}+\frac{RL}{EJx}+\frac{R+L}{kb}\right)^2 \end{pmatrix}^{-1}$$

$$S_{x_3}$$

$$\begin{pmatrix} 1/3\left(-1/3\frac{L^3}{EJy}-\frac{RL(R+L)}{EJy}-krx^{-1}-\frac{(R+L)^2}{kbt}\right)\left(\frac{L}{EJy}+kbt^{-1}\right)Ty\left(-1/2\frac{L^2}{EJy}-\frac{RL}{EJy}+-\frac{-R-L}{kbt}\right) \\ -1/3Fx\left(1/3\frac{L^3}{EJy}+\frac{RL(R+L)}{EJy}+krx^{-1}+\frac{(R+L)^2}{kbt}\right)\left(\frac{L}{EJy}+kbt^{-1}\right) \\ \cdot\left(\frac{L}{EA}+ka^{-1}\right)+1/3\left(1/3\frac{L^3}{EJy}+\frac{RL(R+L)}{EJy}+krx^{-1}+\frac{(R+L)^2}{kbt}\right)\sqrt{3}\left(\frac{L}{EJy}+kbt^{-1}\right)Fz\left(\frac{L}{EA}+ka^{-1}\right) \\ +1/3\left(-1/2\frac{L^2}{EJy}-\frac{RL}{EJy}+\frac{-R-L}{kbt}\right)^3Ty-1/3\left(-1/2\frac{L^2}{EJy}-\frac{RL}{EJy}+\frac{-R-L}{kbt}\right)\left(\frac{L}{EJy}+kbt^{-1}\right)Ty\left(\frac{L}{EA}+ka^{-1}\right) \end{pmatrix}$$

$$\begin{pmatrix} -\left(-1/2\frac{L^2}{EJy}-\frac{RL}{EJy}+\frac{-R-L}{kbt}\right)^2+\left(1/3\frac{L^3}{EJy}+\frac{RL(R+L)}{EJy}+krx^{-1}+\frac{(R+L)^2}{kbt}\right)\left(\frac{L}{EJy}+kbt^{-1}\right) \\ +\left(\frac{L}{EJy}+kbt^{-1}\right)\cdot\left(\frac{L}{EA}+ka^{-1}\right) \end{pmatrix}^{-1}\left(1/3\frac{L^3}{EJy}+\frac{RL(R+L)}{EJy}+krx^{-1}+\frac{(R+L)^2}{kbt}\right)^{-1}$$

$$S_{y_3}$$

$$\begin{pmatrix} -1/3\left(1/2\frac{L^2}{EJx}+\frac{RL}{EJx}+\frac{R+L}{kb}\right)\sqrt{3}\left(\frac{L}{JpG}+kt^{-1}\right)Tz+1/3\left(1/3\frac{L^3}{EJx}+\frac{RL(R+L)}{EJx}+kry^{-1}+\frac{(R+L)^2}{kb}\right)Fy\left(\frac{L}{JpG}+kt^{-1}\right) \\ +1/3\left(\frac{L}{EJx}+kb^{-1}\right)\left(1/3\frac{L^3}{EJx}+\frac{RL(R+L)}{EJx}+kry^{-1}+\frac{(R+L)^2}{kb}\right)Fy-1/3Fy\left(1/2\frac{L^2}{EJx}+\frac{RL}{EJx}+\frac{R+L}{kb}\right)^2 \\ +1/3\left(1/2\frac{L^2}{EJx}+\frac{RL}{EJx}+\frac{R+L}{kb}\right)Tx\left(\frac{L}{JpG}+kt^{-1}\right) \end{pmatrix}$$

$$\begin{pmatrix} \left(1/3\frac{L^3}{EJx}+\frac{RL(R+L)}{EJx}+kry^{-1}+\frac{(R+L)^2}{kb}\right)\cdot\left(\frac{L}{JpG}+kt^{-1}\right)+\left(\frac{L}{EJx}+kb^{-1}\right)\left(1/3\frac{L^3}{EJx}+\frac{RL(R+L)}{EJx}+kry^{-1}+\frac{(R+L)^2}{kb}\right) \\ -\left(1/2\frac{L^2}{EJx}+\frac{RL}{EJx}+\frac{R+L}{kb}\right)^2 \end{pmatrix}^{-1}$$

$$S_{z_3}$$

$$\begin{pmatrix} -1/3\left(\frac{L}{EJy}+kbt^{-1}\right)Fz\left(1/3\frac{L^3}{EJy}+\frac{RL(R+L)}{EJy}+krx^{-1}+\frac{(R+L)^2}{kbt}\right)-1/3\sqrt{3}\left(\frac{L}{EJy}+kbt^{-1}\right)Fx\left(1/3\frac{L^3}{EJy}+\frac{RL(R+L)}{EJy}+krx^{-1}+\frac{(R+L)^2}{kbt}\right) \\ +1/3\left(-1/2\frac{L^2}{EJy}-\frac{RL}{EJy}+\frac{-R-L}{kbt}\right)^2Fz+1/3\sqrt{3}\left(-1/2\frac{L^2}{EJy}-\frac{RL}{EJy}+\frac{-R-L}{kbt}\right)^2Fx \end{pmatrix}$$

$$\left(-\left(-1/2\frac{L^2}{EJy}-\frac{RL}{EJy}+\frac{-R-L}{kbt}\right)^2+\left(1/3\frac{L^3}{EJy}+\frac{RL(R+L)}{EJy}+Krx^{-1}+\frac{(R+L)^2}{kbt}\right)\left(\frac{L}{EJy}+kbt^{-1}\right)+\left(\frac{L}{EJy}+kbt^{-1}\right)\left(\frac{L}{EA}+ka^{-1}\right)\right)^{-1}$$

$$M_{x_3}$$

$$\begin{pmatrix} -1/3Tx\left(\frac{L}{JpG}+kt^{-1}\right)\left(1/3\frac{L^3}{EJx}+\frac{RL(R+L)}{EJx}+kry^{-1}+\frac{(R+L)^2}{kb}\right)\left(\frac{L}{EJx}+kb^{-1}\right) \\ +1/3\sqrt{3}\left(\frac{L}{JpG}+kt^{-1}\right)Tz\left(\frac{L}{EJx}+kb^{-1}\right)\left(1/3\frac{L^3}{EJx}+\frac{RL(R+L)}{EJx}+kry^{-1}+\frac{(R+L)^2}{kb}\right) \\ -1/3\left(\frac{L}{EJx}+kb^{-1}\right)\left(1/3\frac{L^3}{EJx}+\frac{RL(R+L)}{EJx}+kry^{-1}+\frac{(R+L)^2}{kb}\right)Fy\left(1/2\frac{L^2}{EJx}+\frac{RL}{EJx}+\frac{R+L}{kb}\right) \\ -1/3\left(1/3\frac{L^3}{EJx}+\frac{RL(R+L)}{EJx}+kry^{-1}+\frac{(R+L)^2}{kb}\right)Fy\left(\frac{L}{JpG}+kt^{-1}\right)\cdot\left(1/2\frac{L^2}{EJx}+\frac{RL}{kb}\right)+1/3Fy\left(1/2\frac{L^2}{EJx}+\frac{FL}{EJx}+\frac{R+L}{kb}\right)^3 \end{pmatrix}$$

$$\left(\frac{L}{EJx}+kb^{-1}\right)^{-1}\begin{pmatrix} \left(1/3\frac{L^3}{EJx}+\frac{RL(R+L)}{EJx}+kry^{-1}+\frac{(R+L)^2}{kb}\right)\left(\frac{L}{JpG}+kt^{-1}\right) \\ +\left(\frac{L}{EJx}+kb^{-1}\right)\cdot\left(1/3\frac{L^3}{EJx}+\frac{RL(R+L)}{EJx}+kry^{-1}+\frac{(R+L)^2}{kb}\right)-\left(1/2\frac{L^2}{EJr}+\frac{RL}{EJr}+\frac{R+L}{kb}\right)^2 \end{pmatrix}^{-1}$$

$$M_{y_3}$$

$$\left(\begin{array}{l} 1/3\left(1/3\frac{L^3}{EJy}+\frac{RL(R+L)}{EJy}+krx^{-1}+\frac{(R+L)^2}{kbt}\right)\left(\frac{L}{EJy}+kbt^{-1}\right)Ty+1/3\left(\frac{L}{EJy}+kbt^{-1}\right)Ty\left(\frac{L}{EA}+ka^{-1}\right) \\ -1/3Ty\left(-1/2\frac{L^2}{EJy}-\frac{RL}{EJy}+\frac{-R-L}{kbt}\right)^2-1/3\sqrt{3}\left(-1/2\frac{L^2}{EJy}-\frac{RL}{EJy}+-\frac{R-L}{kbt}\right)\left(\frac{L}{EA}+ka^{-1}\right)Fz \\ +1/3\left(-1/2\frac{L^2}{EJy}-\frac{RL}{EJy}+\frac{-R-L}{kbt}\right)Fx\left(\frac{L}{EA}+ka^{-1}\right) \end{array}\right)$$

$$\left(-\left(-1/2\frac{L^2}{EJy}-\frac{RL}{EJy}+\frac{-R-L}{kbt}\right)^2+\left(1/3\frac{L^3}{EJy}+\frac{R(R+L)}{EJy}+krx^{-1}+\frac{(R+L)^2}{kbt}\right)\cdot\left(\frac{L}{EJy}+kbt^{-1}\right)+\left(\frac{L}{EJy}+kbt^{-1}\right)\left(\frac{L}{EA}+Ka^{-1}\right)\right)^{-1}$$

$$M_{-z_3}$$

$$\left(\begin{array}{l} -1/3\left(\frac{L}{EJx}+kb^{-1}\right)\left(1/3\frac{L^3}{EJx}+\frac{RL(R+L)}{EJx}+kry^{-1}+\frac{(R+L)^2}{kb}\right)Tz+1/3\left(1/2\frac{L^2}{EJx}+\frac{RL}{EJx}+\frac{R+L}{kb}\right)^2Tz \\ +1/3\left(\frac{L}{EJx}+kb^{-1}\right)\left(1/3\frac{L^3}{EJr}+\frac{RL(R+L)}{EJx}+kry^{-1}+\frac{(R+L)^2}{kb}\right)\cdot\sqrt{3}Tx+1/3\sqrt{3}\left(1/2\frac{L^2}{EJx}+\frac{RL}{EJx}+\frac{R+L}{kb}\right)^2Tx \end{array}\right)$$

$$\left(\begin{array}{l} \left(1/3\frac{L^3}{EJx}+\frac{RL(R+L)}{EJx}+kry^{-1}+\frac{(R+L)^2}{kb}\right)\left(\frac{L}{JpG}+kt^{-1}\right)+\left(\frac{L}{JpG}+kt^{-1}\right) \\ \quad +\left(\frac{L}{EJx}+kb^{-1}\right)\left(1/3\frac{L^3}{EJx}+\frac{RL(R+L)}{EJx}+kry^{-1}+\frac{(R+L)^2}{kb}\right)-\left(1/2\frac{L^2}{EJx}+\frac{RL}{EJx}+\frac{R+L}{kb}\right)^2 \end{array}\right)^{-1}$$

References

1. Fischer U, Zimmermann C, Jörg W (2002) SG-Balance 192-6I calibration report. RUAG Center Aerodynamics
2. http://www.windtunnel.soton.ac.uk/balance/balance_ RJMitchell.html University of Southampton, 2010. Accessed 4/2010
3. http://www.mmtool.com/balances.html Modern machine & tool CO., INC, Strain Gage Wind Tunnel Balances, 2010. Accessed 4/2010
4. http://www.ruag.com RUAG Aerospace Defence Technology, Strain Gauge Balances for Wind Tunnel Measurements, 2005. Accessed 4/2010
5. Carignan F et al (1985) Force measuring platform and load cell using strain gages to measure shear forces, Advanced Mechanical Technology, Inc., Patent US4493220
6. Spletzer B, Marron L (2000) Information package for the simplified six-axis load cell. Sandia National Laboratories, January, e-mail: blsplet @sandia.gov
7. BermeN (2002) Multi-component force and moment measuring platform and load transducer. Bertec Corporation, Patent US6354155
8. Blakeborough A, Clément D, Williams MS, Woodward N (2002) Novel load cell for measuring axial force, shear force, and bending movement in large-scale structural experiments. Exp Mech 42(1):115–122
9. Engeler P et al (1995) Multicomponent force and moment measuring arrangement. K.K. Holding AG, US5402684
10. Meyer R et al (1998) Six axis load cell. MTS SYSTEMS CORPORATION, European Patent EP0632884B1
11. Gobbi M, Mastinu G, Giorgetta F (2005) Sensors for measuring forces and moments with application to ground vehicle design and engineering. Proceedings ASME IMECE, paper n. IMECE2005-81143
12. http://www.amti.biz/ Advanced Mechanical Technology, Inc, 2010. Accessed 4/2010
13. http://www.jr3.com/ Multi-axis load cell technologies, 2010. Accessed 4/2010
14. Yee AG, Akeel HA (1996) Six axis force sensor employing multiple shear strain gages. Fanuc USA Corporation (Elkgrove Village, IL), United States Patent 5490427
15. Meyer RA, Olson DJ (1994) Six axis load cell. MTS Systems Corporation (Eden Prairie, MN), United States Patent 5315882
16. Liu H, Willberg B, Meusel P (2005) Force moment sensor. Deutsches Zentrum fur Luft-und Raumfahrt e.V. (Koln, DE), United States Patent 6871552
17. Berme N (2002) Multi-component force and moment measuring platform and load transducer. Bertec Corporation (Worthington, OH), United States Patent 6354155

18. Meyer RA, Olson DJ (2005) Multi-axis load cell. MTS Systems Corporation (Eden Prairie, MN), United States Patent 6845675
19. Meyer, RA, Kempainen AJ, Olson DJ (2004) Multi-axis load cell body. MTS Systems Corporation (Eden Priarie, MN), United States Patent 6769312
20. Lerat B (1989) Transducer for bending and twisting moments. Commissariat A L'Energie Atomique, Patent US4879913
21. Wensink H, de Boer MJ, Wiegerink RJ, Zwijze AF, Elwenspoek MC (1998) First micromachined silicon load cell for loads up to 1000 kg. Proc. SPIE '98, vol. 3514 Micromachined Devices and Components IV
22. Zwijze AF, Wiegerink RJ, Lammerink TSJ, Elwenspoek MC (1998) Low creep and hysteresis load cell based on a force to liquid pressure transformation. Proceedings of the Dutch National Sensor Conference, Enschede, pp 287–292, March 2
23. Byun Y et al (2002) Parallel type six-axes force moment measuring apparatus. Samsung Electronics Co., Ltd., Patent US6349604
24. http://www.ati-ia.com/ ATI Industrial Automation, (Series OMEGA and GAMMA), 5/2005
25. Mastinu G, Gobbi M (2006) Giunto elastico a cerniera sferica traslante e sensore di forze e momenti perfezionato con tale giunto. Italian Patent, ME.05.025.A, 22 May 2006
26. Mastinu G, Gobbi M (2003) Dispositivo e metodo per la misura di forze e momenti. Italian Patent MI2003A 001500, 22 July 2003
27. Mastinu G, Gobbi M (2005) Device and method for measuring forces and moments. Patent WO2005015146, 17 February 2005
28. Mastinu G, Gobbi M (2007) Elastic joint with translating spherical hinge and force and moment sensor improved by means of the said joint. International Application number PCT/IB2007/001335, 16 May 2007
29. Gobbi M, Mastinu G, Pennati M (2007) Indoor testing of road vehicle suspensions. Meccanica 43(2):173–184. doi:10.1007/s11012-008-9119-5, 28 February 2008
30. Cook H, Carignan FJ, White BF (1999) Multi-axis wheel transducer with angular position detector. Advanced Mechanical Technology, Inc. Patent, US5886350
31. http://www.sendev.com/ Sensor Development Inc. (Model 77016 and 6 axis WFS), 5/2005. Accessed 4/2010
32. http://www.michsci.com/ Michigan Scientific Corporation (model LW 12.8), 5/2005. Accessed 4/2010
33. http://www.mts.com/ MTS Systems Corporation (SWIFT Wheel Force Transducer), 5/2005. Accessed 4/2010
34. http://www.kistler.com Kistler (RoaDyn Wheel Force Sensor), 5/2005. Accessed 4/2010
35. http://www.igel-ingenieure.de/ (IGel WFT Wheel Sensor), 5/2005. Accessed 4/2010
36. Giorgetta F, Gobbi M, Mastinu G (2007) On the testing of vibration performances of road vehicle suspensions. Exp Mech 47:485–495. doi:10.1007/s11340-006-9022-8
37. Gobbi M, Mastinu G (2004) Wheels with integrated sensors for measuring tyre forces and moments. Proc. of the AVEC 04 Symposium, Arnhem, August
38. Gobbi M, Previati G, Guarneri P, Mastinu G (2010) A new six-axis load cell. Part II: error analysis, construction and experimental assessment of performances. Exp Mech, xxx, DOI xxx